Anal. Methods Environ. Chem. J. 6 (3) (2023) 67-88

AMECJ

Research Article, Issue 3
Analytical Methods in Environmental Chemistry Journal
Journal home page: www.amecj.com/ir

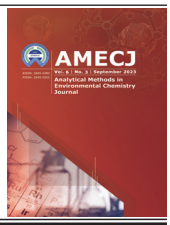

Analytical study on lead elimination by anionic clays: Characterization, adsorption kinetics, isotherm, thermodynamic, mechanism and adsorption

Salah Bahah[a,b,*]

[a] *Department of Environmental Engineering, Faculty of Science and Technology, University Bachir El Ibrahimi of Bordj Bou Arreridj, Algeria.*

[b] *Laboratory of Chemical Processes Engineering (LGPC), Department of Process Engineering, Faculty of Technology, University Ferhat Abbas Setif19000 ,1- Sétif, Algeria.*

ARTICLE INFO:

Received 20 May 2023
Revised form 30 Jul 2023
Accepted 19 Aug 2023
Available online 30 Sep 2023

Keywords:
Anionic clays,
Lead,
Adsorption,
Co-precipitation,
Functional groups

ABSTRACT

The co-precipitation method synthesized the synthetic anionicMg–Al and Ni-Al clays with three molar ratios (Mg/Al, Ni/Al). The samples were characterized by powder X-ray diffraction (XRD), Fourier transform infrared spectroscopy (FTIR), and scanning electron microscopy (SEM). No other crystalline phases were detected in the powder XRD patterns of the co-precipitated samples. The infrared spectra obtained all the functional groups that characterize these two types of anionic clays. SEM micrographs indicate the presence of particles and aggregates. The particles, or aggregates, are in the form of plates, supported by particles of acceptable sizes. The optimal pH for maximum lead adsorption is about 6.5 for both clays. The optimal adsorbent masses for the maximum percentages of lead removal are 0.2 g for Mg_3AlCO_3 and 0.25 g for Ni_3AlCO_3. The Mg_3AlCO_3 has a maximum adsorption capacity of lead, where q_m=73.42 mg g^{-1}. The adsorbed amount increases with increasing temperature for both types of clays studied. The equilibrium time of Pb^{2+} adsorption is reached after 5 min for both clays. The most appropriate models to describe the experimental data of adsorption kinetics and isotherms are pseudo-second-order and Langmuir. The detection limit (LOD) was 0.272 mg L^{-1}. The linearity range was 1 to 5 mg L^{-1}; the correlation coefficient in this range was 0.9997.

1. Introduction

Anionic clays, or Layered Double Hydroxides (LDHs), are mixed metal hydroxides that have a general formula expressed as$[(M^{II})_{1-x}(M^{III})_x(OH)_2]^{x+}(A^{m-}_{x/m})\cdot nH_2O]$. $M^{2+}$is a divalent cation (typically Mg, Zn, Ni, Co), $M^{3+}$is a trivalent metal cation (Al, Fe, Cr), A^{n-} is a charge anion, n/x is the molar ratio between di and trivalent cations, $M^{2+}/(M^{2+} + M^{3+})$, and m, the number of water molecules[1-3]. The structure of these clays consists of positively charged mixed metal hydroxide layers separated by charge-balancing anions and water molecules [4]. The cationic sheets containing $M(OH)_2$ in octahedral surroundings are linked by three edges, as in the brucite structure, between which compensating layers of anions are found [5]. These compounds have been the subject of much interest and research in recent years thanks to their interesting properties of anionic exchange [6,7], adsorption and porosity, which make it possible to envisage the intercalation of a large variety of anions (organic or inorganic)

*Corresponding Author: Salah Bahah
Email: basalah.univ@gmail.com
https://doi.org/10.24200/amecj.v6.i03.248

and the immobilization of various species, giving these hybrid materials a particular reactivity [6,7]. Therefore, LDH is considered a promising material [8]. Heavy metals are one of the main categories of water pollution; these releases pose a real danger to humans and their environment due to their stability and low biodegradability [9-11]. The use of the adsorption technique to remove heavy metals in aqueous solutions on different solid supports, especially on new materials such as anionic clays, has been the subject of much work [3, 5, 12]. Among the scientific results that use layered double hydroxides as adsorbents to remove lead are the studies of Yasin et al. (2014) [13]. The types of LDHs used to remove lead (Pb) from the aqueous solution are MgAl-NO_3 and Tartrate-MgAl. In this study, the maximum lead adsorption capacity calculated by the Langmuir model is 8.4 and 3.2 mg g^{-1} for Tartrate-MgAl and $MgAlNO_3$, respectively [13]. Yanming et al. (2017) [14] studied the removal of Pb^{2+} ions from an aqueous solution by glutamate intercalated in layered double hydroxide. The maximum retention capacity of Pb^{2+} is 68.49 mg g^{-1} [14]. The concentration of Pb and other metal ions can be determined by several techniques, which can be grouped under atomic spectrometry. Graphite furnace atomic absorption spectrophotometer (GF-AAS) is the best technique method. Several research studies use this technique to determine the lead concentration in the blood, like studies of Pacer et al. (2022) [15]. In addition, GF-AAS is an excellent method currently applied for trace lead concentration with high accuracy and precision [15, 16]. Like GF-AAS, inductively coupled plasma mass spectrometry and ICP-MS is other assay technique with precise and accurate results. However, it is a simple and rapid method compared to ICP-MS [17]. The comparative study carried out by Trzcinka-Ochocka et al. for the determination of lead and cadmium shows that validation parameters for ICP-MS and GF-AAS were similar. However, ICP-MS for Pb determinations is better than GF-AAS. Also, the detection limits (LOD) of ICP-MS are better than GF-AAS for lead analysis [18]. Inductively Coupled Plasma -Atomic Emission Spectroscopy (ICP-AES), sometimes named ICP-optical emission spectrometry (ICP-AES), is a device that results from the coupling between a high-frequency induced argon plasma and a spectrometer, which is used to calculate the concentration of metals in solid, liquid or gas samples. The LOD of the ICP-AES technique is lower than ICP-MS [19]. In addition, there are other lead dosage techniques without spectroscopic techniques, such as cyclic voltammetry (CV). Riyanto et al. showed that the electroanalysis method for lead determination in wastewater is accurate, precise, reproducible and inexpensive, with acceptable correlation [20]. Compared with spectroscopic techniques, the LOD of electroanalysis (0.929 mg L^{-1}) is higher than that of spectroscopic methods.

In this paper, lead removal from an aqueous solution was performed using two-layered double hydroxides, namely Mg_3AlCO_3 and Ni_3AlCO_3. The co-precipitation method prepared these two adsorbents with a molar ratio of (Mg/Al) equal to 3. Ni_3AlCO_3 can be considered among the LDHs not used to eliminate heavy metals from aqueous solution. The adsorption capacities of lead with two anionic clays at room temperature in optimized pH were compared and analyzed. We studied the effect of different parameters such as the Ni/Al ratio, pH, contact time, dose of adsorbent and temperature in the adsorption of Pb^{2+} ions from an aqueous solution. In addition, the mechanism and thermodynamic parameters were studied.

2. Experimental

2.1. Reagents and Materials

The products of magnesium nitrate hexahydrate ($Mg(NO_3)_2.6H_2O$; CAS 13446-18-9; Molecular Weight 256.41), Aluminum nitrate nonahydrate ($Al(NO_3)_3.9H_2O$; CAS Number: 7784-27-2; M. W.: 375.13) and Nickel nitrate hexahydrate ($Ni(NO_3)_2.6H_2O$; CAS 13478-00-7; Molecular Weight 290.79) used for the synthesis of $MgAlCO_3$ and $NiAlCO_3$ were purchased from Sigma, Germany. Sodium carbonates ($NaCO_3$), Sodium hydroxide (NaOH) and Lead nitrate $Pb(NO_3)_2$ were purchased from Merck.

2.2. Apparatus

The absorption measurements were made with AA-6200 Atomic Absorption Flame Emission Spectrophotometer SHIMADZU. Calibrating standard lead solutions were prepared by dilution from the stock solution (1000 mg L^{-1}). The linear working range was obtained between 1 to 5 mg L^{-1}. To estimate the sensitivity of the FAAS method, we calculated the limit of detection (LOD) and the limit of quantification (LOQ). The LOD and LOQ values were achieved at 0.272 mg L^{-1} and 0.825 mg L^{-1}, respectively.

2.3. Synthesis method

The LDHs studied are $NiAlCO_3$ (R=2, 3 et 4) and $MgAlCO_3$ (R=3). These clays were synthesized by the direct co-precipitation method, in which an aqueous solution containing appropriate amounts of nitrate elements (hydrated metal salts as sources) was added dropwise into an alkaline solution of Na_2C0_3 and NaOH at room temperature under vigorous stirring. During the synthesis, the pH was adjusted to pH 10. The resulting suspension was stirred for 18 hours at 65 °C. After cooling to room temperature, the precipitate was centrifuged and washed several times with bi-distilled water until there was no trace of nitrate ($AgNO_3$ test) and then dried overnight in an oven at 100 °C.

2.4. Adsorption method

The study of the adsorption of lead was performed by the batch method. The lead stock solution was prepared by dissolving Pb $(NO_3)_2$ in distilled water and diluting it to the desired concentration. Adsorption of Pb^{2+} on the selected clay was carried out in a 50 ml conical flask by taking 50 ml of a solution of the desired Pb^{2+} concentration to which 200 mg of the adsorbent was added. The adsorbate in the mixture was separated by centrifugation. An atomic absorption spectrophotometer determined the residual Pb2+ in the filtrate. All experiments except the pH variation study were performed at the stock solution pH. In the case of pH variation studies, a variable concentration of diluted NaOH and HCl solutions was used to adjust the pH. Figure 1 presents the adsorption method.

The adsorption of lead was calculated by Equation 1.

$$q_e = \frac{C_i - C_e}{m} * V \qquad \text{(Eq.1)}$$

Where q_e= lead adsorbed (mgg^{-1}); V = solution volume (L); C_i = initial concentration (mg $Pb^{2+}L^{-1}$); Ce (mgPb^{2+} L^{-1}) =equilibrium concentration and m adsorbent mass. % Removal of metal ions were calculated using Equation 2.

$$\text{Removal} = \frac{C_i - C_e}{C_i} * 100 \qquad \text{(Eq. 2)}$$

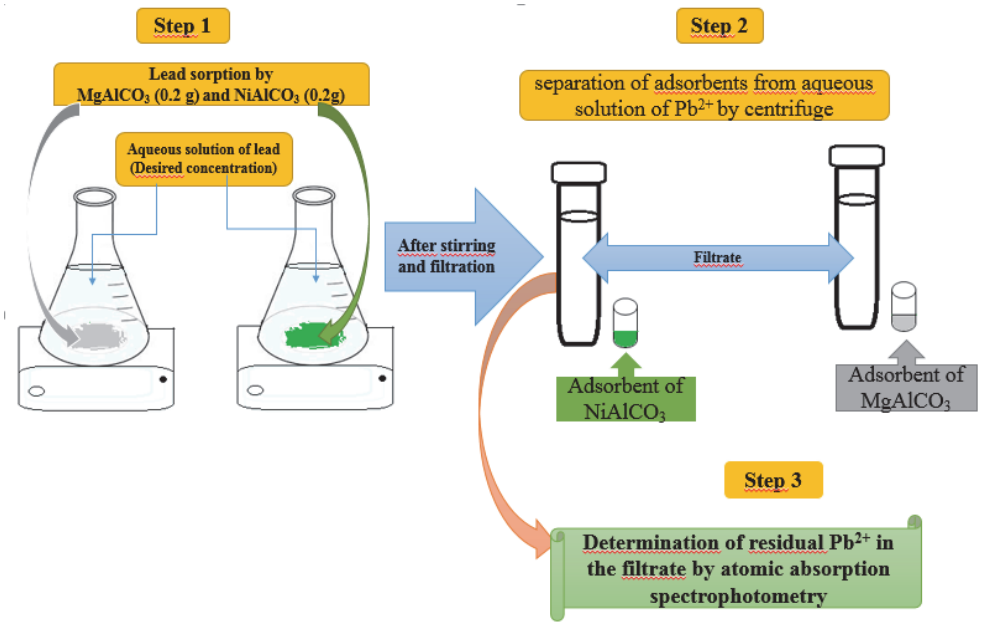

Fig. 1. Adsorption of lead by a batch method

3. Results and Discussion

3.1. Characterization

A Bruker D8 diffractometer with CuKα radiation (λ= 0.15406 nm) was used to study the structural properties of the clay. A scanning electronic microscopy instrument (S-4800), a Hitachi model (Japan), was utilized to study the surface properties. Fourier transform infrared spectroscopy (Perkin-Elmer model; USA) was applied to study the functional group of the adsorbent. Moreover, this last technique was used to examine the effect of the adsorption of Pb^{2+} on the different bands of the functional groups after adsorption. The infrared spectra were carried out between 4000 cm^{-1} and 400 cm^{-1}.

3.1.1.Characterization by XRD

The X-ray diffraction patterns of the prepared phases (Fig. 2a and 2b) are characteristic of layered double hydroxide materials (LDHs). Peaks 003 and 006 are sharp, narrow, and symmetric; the baseline is low and stable, which indicates a high degree of crystallinity and a typical structure of anionic clays. These reflections correspond to the layer order along the c-axis [21]. Inter-reticular distances are 7.70 °A and 7.75 °A for Ni/Al (R=3) and Mg/Al (R=3), respectively. These values are in order of those reported in similar studies by Kristina Klemkaite et al. [22]and Faour et al. [23]. The cell parameters of Ni_3AlCO_3 and $Mg_3AlCO_{3,}$ calculated as a = $2*d_{110}$ [24], are 3.04 and 3.06 °A, respectively. The constant c calculated using the equation $c=3*d_{003}$ [25] shows that the corresponding values for Ni_3AlCO_3 and Mg_3AlCO_3 are (23.10 °A) and (23.25 °A), respectively. These values always agree with those of Kristina Klemkaite et al. [22] and Faour et al. [23].

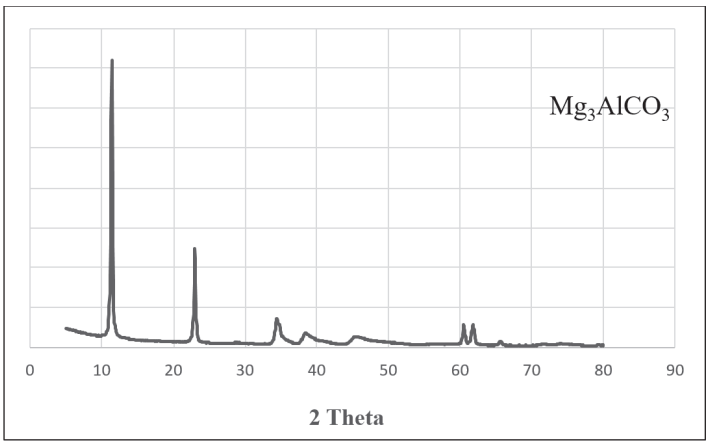

Fig. 2a. XRD patterns of Mg_3 Al–CO_3

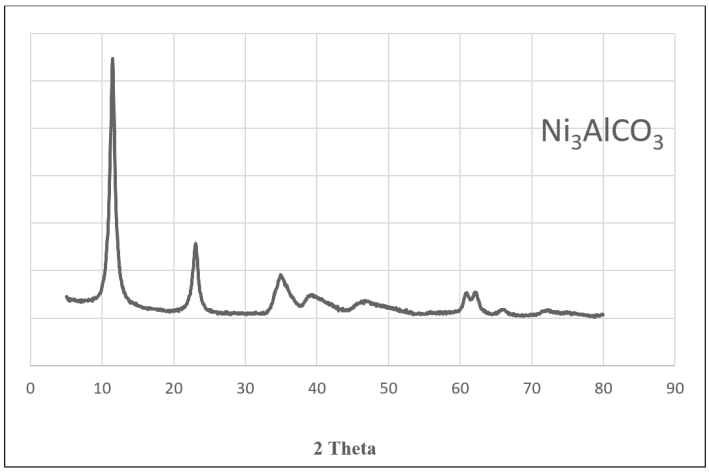

Fig. 2b. XRD patterns of Ni_3Al–CO_3.

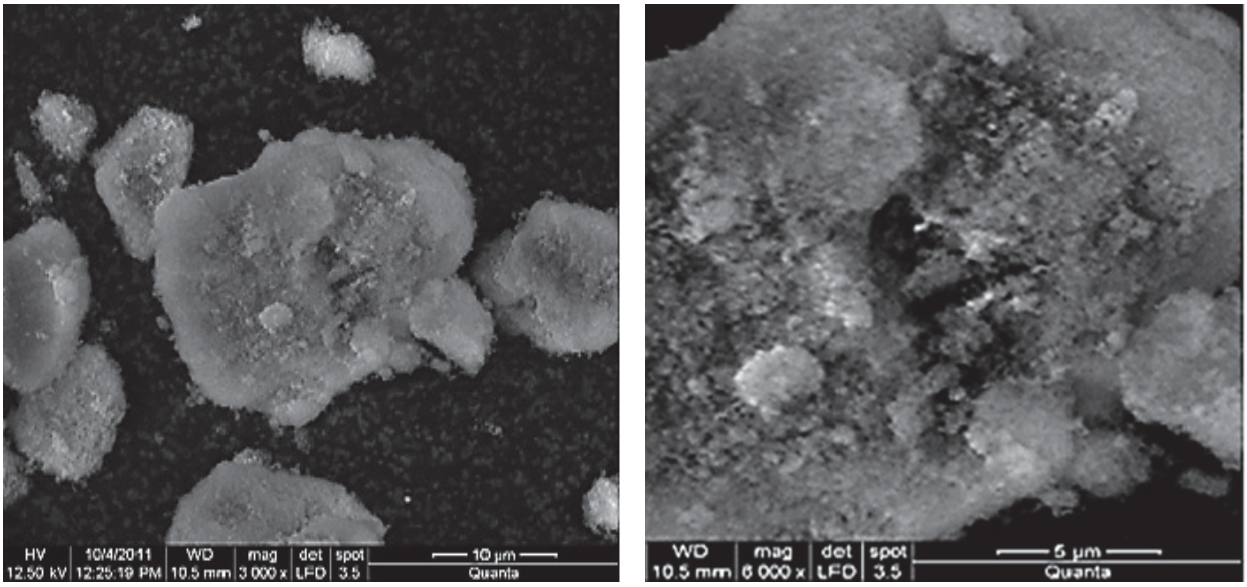

Fig. 3a. The SEM micrograph of (a) $Ni_3Al–CO_3$ (R=3)

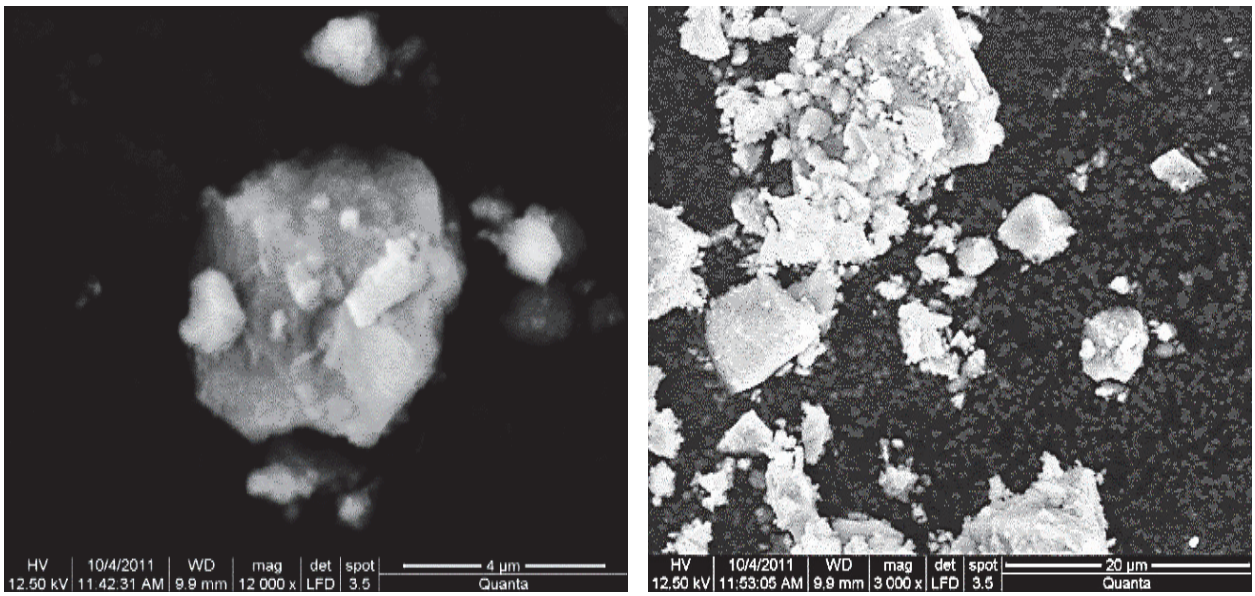

Fig. 3b. The SEM micrograph of $Mg_3Al–CO_3$(R=3).

3.1.2.Characterization by SEM

The images characterizing the surfaces of the different substrates are presented in Figure3a and 3b. The images at different magnifications show surfaces with large porosities and different types and sizes. The large inter-particle pores are occupied by particles of smaller sizes for both clays, which indicate the presence of inter-particle attraction forces that form large aggregates. The particles, or aggregates, are in the form of plates, supported by particles of acceptable sizes. Mg_3AlCO_3 particles are characterized by a rigid (compact) perimeter surrounding a highly porous surface.

3.2. Parameters of adsorption

In the following, we studied the effect of some parameters on lead adsorption, such as the solution's initial pH, the adsorbent's mass, contact time, molar ratio, and temperature. The concentration and volume of the aqueous lead solution were fixed at 50 mgL^{-1} and 50 mL, respectively, and the stirring speed was set at 400 rpm.

3.2.1.Effect of pH

To find the optimal pH corresponding to the maximum adsorption of lead in the aqueous solution, we studied the effect of this factor on the retention of Pb^{2+} at different pHs (from pH 3 to pH 9). The results obtained are shown in Figure 4. The amount retained as a function of the pH solution was determined from the concentration of Pb^{2+} remaining in the solution after equilibrium by the atomic absorption technique. According to Figure 4, the curves can be divided as a function of pH into two regions: the first one represents the domain of pH lower than 6.5 in which the percentage removal of Pb^{2+} retained on the selected anionic clays increases as the pH increases, reaching a maximum value at pH 6.5. At this optimum pH, the lead removal percentages are 95.4% and 81.34% for Mg_3AlCO_3 and Ni_3AlCO_3, respectively. The increase in Pb^{2+} adsorption on both types of LDHs with increasing pH can be explained by the decrease in H^+ ion concentration with increasing pH. Where the clay surface at low pH became positively charged due to the protonation reaction on the surfaces (formation of SOH^{2+}) [25], which leads to repulsive forces between Pb^{2+} ions and SOH^{2+}groups on the adsorbent surface [26]. According to Donglin Zhao, at pH values below 7, lead ions are present as Pb^{2+} in the solution. The adsorption reactions are surface complexation reactions, including two surface reactions. The chemical bonding reaction occurs between the metal ions and the surface functional groups, forming surface complexes of the inner sphere. In the second region, an electrostatic binding reaction occurs between metal ions and oppositely charged surface functional groups, forming surface complexes of the outer sphere at some distance from the surface. The complex adsorption of lead on LDH samples can be described as follows [25,26].

$$Sur\text{-}O^- + Pb^{2+} \rightarrow Sur\text{-}O^-\text{-}Pb^+ + H^+$$

Chemical binding adsorption

$$Sur\text{-}O^- + Pb^{2+} \rightarrow Sur\text{-}O^-\text{----}Pb^{2+}$$

Electrostatic binding adsorption

At pH greater than 6.5, for Mg_3AlCO_3, there is a slight decrease and then stability for lead removed until pH 9. These results almost agree with those found by Donglin Zhao et al., who used anionic clay based on Mg_2Al-LDH to remove lead [26]. For the anionic clay based on Ni_3AlCO_3, the characteristic curve shows a remarkable decrease in the amount of lead removed. At this pH range (pH > 6.5), according to ZHAO, Donglin et al. (2011) [26], lead in the aqueous solution takes the forms of Pb (OH) and Pb $(OH)_2$. Thus, the adsorption of Pb^{2+} on both LDHs occurred by precipitation reaction, as explained by several authors in this pH range (pH > 7) [26]. According to our results, it can be noted that the lead precipitation reaction is better catalyzed on the Mg_3AlCO_3 surface than that of Ni_3AlCO_3, where the amount adsorbed by Mg_3Al remains constant from pH 7.5 and higher compared to Ni_3Al-based clays, where the amounts of lead are decreased with the increase of pH (Figure 4).On the other hand, LIANG, Xuefeng et al. [25] conclude that the adsorption of Pb^{2+} on a clay-type Mg_2Al-Cl LDH results mainly from the precipitation induced by the surface. At optimum pH (pH = 6.5), the results show that the order of the quantity of lead retained for the clays used becomes Equation 3.

$$Q_{ads\ (MgAlCO3(R=3)} > Q_{ads\ (NiAlCO3(R=3)} \qquad \text{(Eq. 3)}$$

Whereas, at pH<5.5 (an acidic medium), the percentage of Pb^{2+} removal by Ni_3AlCO_3 HDL is higher than that of Mg_3AlCO_3 HDL, conversely for the pH > 5.5 range. This can be explained by the start of the lead precipitation reaction occurring in parallel with the complexation reaction from pH 5.5 to the optimum pH of 6.5.

3.2.2.Effect of adsorbent quantity

Different amounts of the adsorbent (0.05–0.3 g) were added to other conical flasks containing 50 mL of the aqueous solution of Pb^{2+} (pH 6.5). Figure 5 shows the variations of Pb^{2+} adsorbed amounts as a function of adsorbent mass for the two anionic clays studied with a contact time of 2 hours. The initial adsorbate concentration used is 50 mg L^{-1}. Lead removal percentages increase as the adsorbent

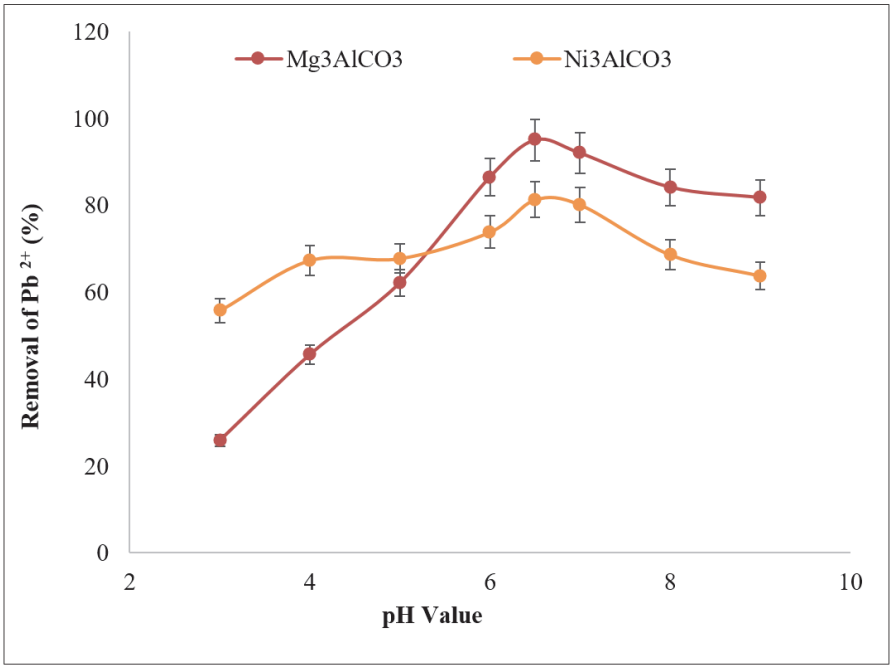

Fig. 4. Effect of initial pH on removal of Pb^{+2} ions onto $Mg3AlCO_3$ and $Ni3AlCO_3$.

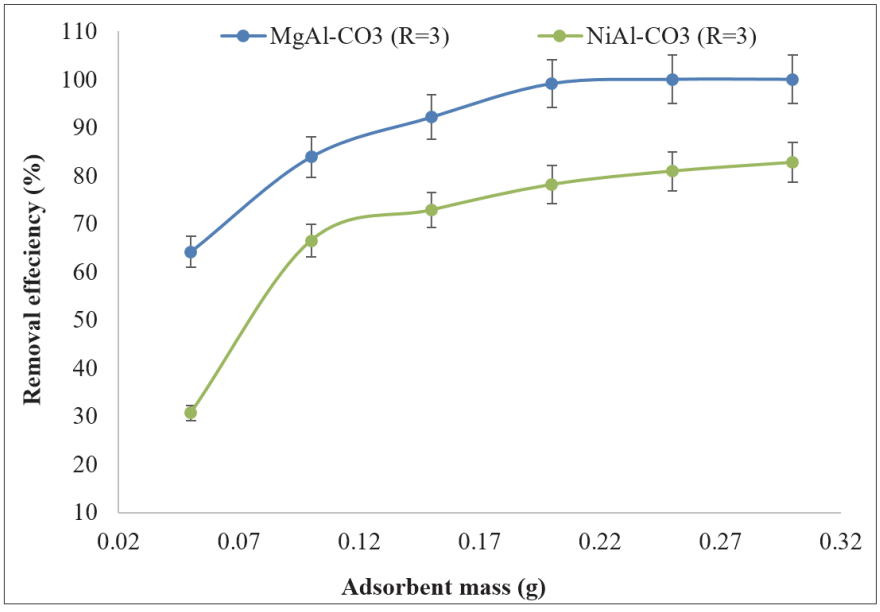

Fig. 5. Effect of mass on the adsorption of Pb^{2+} onto $Ni_3Al\text{-}CO_3$ and $Mg_3Al\text{-}CO_3$

mass increases from 0.05 g to 0.2 g. Above 0.2 g for Mg_3AlCO_3 and 0.25 g for Ni_3AlCO_3, the amount of Pb^{2+} retained remains almost constant regardless of the adsorbent mass. The maximum capacities corresponding to these masses are 95.25 % and 83.66 % for Mg_3AlCO_3 and Ni_3AlCO_3, respectively.

According to Figure 5, the amount of Pb^{2+} was adsorbed on the clays as Equation 4.

Qads (MgAlCO3(95.25%) > Qads (NiAlCO3(83.665) (Eq.4)

3.2.3.Effect of temperature

The effect of temperature on lead adsorption was studied at 20 °C, 30 °C, 40 °C, 50°C, and as well as pH of the solution. Figure 6 shows the percentage of lead removal as a function of temperature for Mg_3AlCO_3 and Ni_3AlCO_3. From the curves shown in Figure 6, the adsorbed amount increases with increasing temperature for both types of LDHs, where the lead removal percentages reach 94.16 % and 85.39 % for Mg_3AlCO_3 and Ni_3AlCO_3, respectively. The percentage of lead removal by Mg_3AlCO_3 is higher than that of Ni_3AlCO_3 for all temperatures. This may indicate that the adsorption of lead onto the active sites of LDHs studied is endothermic [27]. The increase in temperature can be enlarged and activate the adsorbent surface, which facilitates the mobility of lead ions from the bulk solution to the adsorbent surfaces and enhances the accessibility to the adsorbent active sites [27].

3.2.4.Effect of contact time and molar ratio

The study of the contact effect was carried out using four LDHs of the types Mg_3AlCO_3, Ni_2AlCO_3, Ni_3AlCO3, and Ni_4AlCO_3 (to see the molar ratio effect, (R=2, 3, and 4). The mass of the adsorbent used is 0.2 g, the concentration of Pb^{2+} in the solution is 50 mg $Pb^{2+}L^{-1}$, the stirring speed is 400 rpm, and the adsorption occurs at ambient temperature. The equilibration time is an important parameter that allows the determination of the rate of lead elimination, whether it is fast or slow, as well as the evaluation of the effectiveness of the absorbent. The shape of the curves shown in Figure 7 is typical of saturation curves with a slight quantitative difference. The Pb^{2+} retention kinetics consists of two distinct steps: an initial fast step with a contact time of up to 5 minutes for Mg_3AlCO_3 and Ni_3AlCO_3 and about 10 minutes for Ni_2AlCO_3 and Ni_4AlCO_3, respectively, and a slower second step in which retention reaches a plateau, indicating the achievement of balance. The equilibrium times for Ni_2AlCO_3 and Ni_4AlCO_3 represent the double time required for equilibrium compared to Mg_3AlCO_3 and Ni_3AlCO_3. This can be explained by the crystalline factor in Mg_3AlCO_3 and Ni_3AlCO_3, which is good compared to Ni_2AlCO_3 and Ni_4AlCO_3. The regular and repetitive distribution of atoms and functional groups bonded with these atoms, such as OH, facilitate the rapid attachment of Pb^{2+} ions to these surface functional groups. It is known that the elimination of Pb^{2+} for all adsorbents is done under the same conditions (temperature, stirring speed).

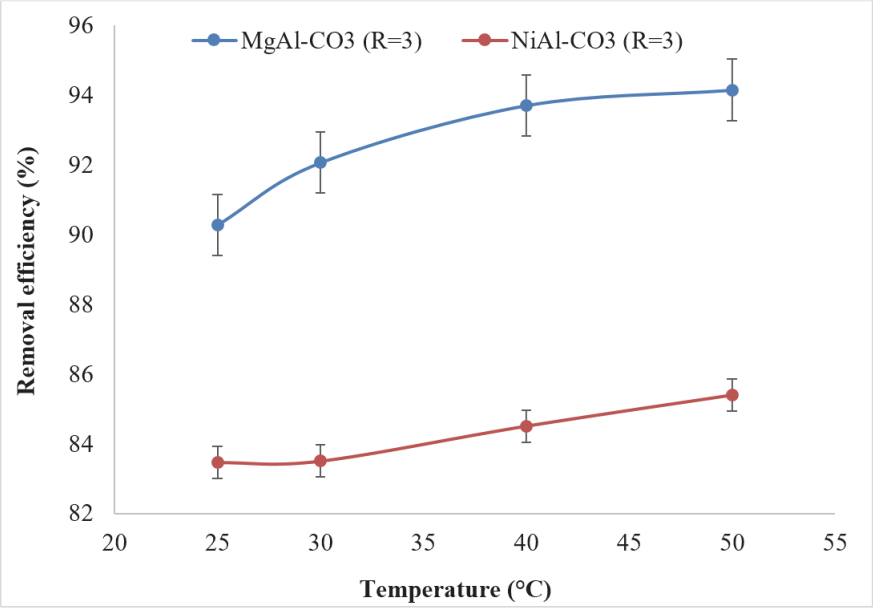

Fig. 6. Effect of temperature on Pb^{2+} adsorption on Mg_3AlCO_3 and Ni3$AlCO_3$

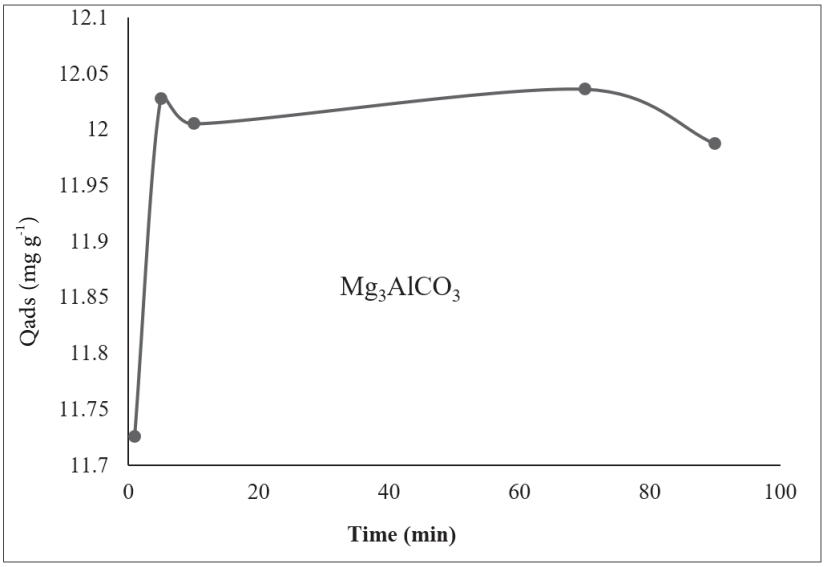
12.1
12.05
12
11.95
11.9
11.85
11.8
11.75
11.7
Qads (mg g-1)
Mg3AlCO3
0
20
40
60
80
100
Time (min)

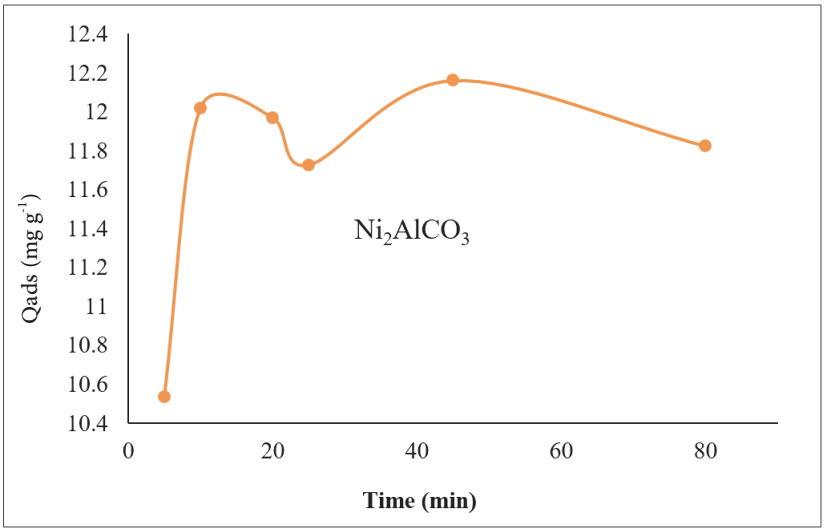
12.4
12.2
12
11.8
11.6
11.4
11.2
11
10.8
10.6
10.4
Qads (mg g-1)
Ni2AlCO3
0
20
40
60
80
Time (min)

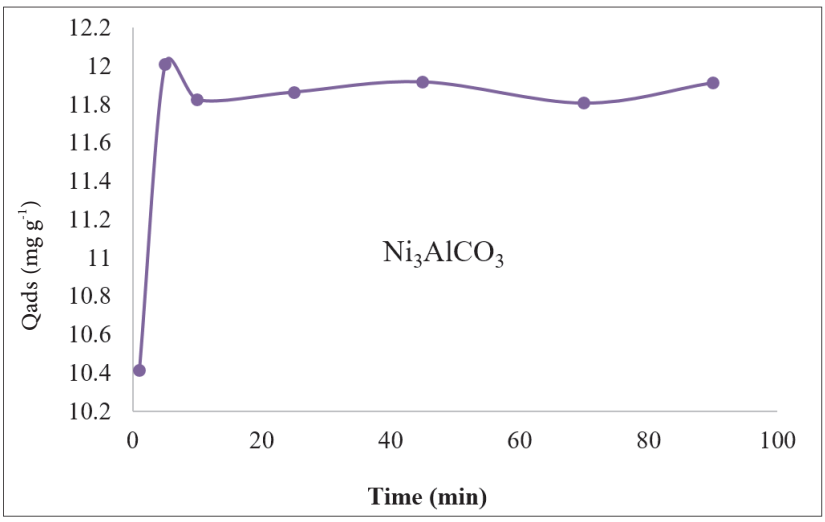
12.2
12
11.8
11.6
11.4
11.2
11
10.8
10.6
10.4
10.2
Qads (mg g-1)
Ni3AlCO3
0
20
40
60
80
100
Time (min)

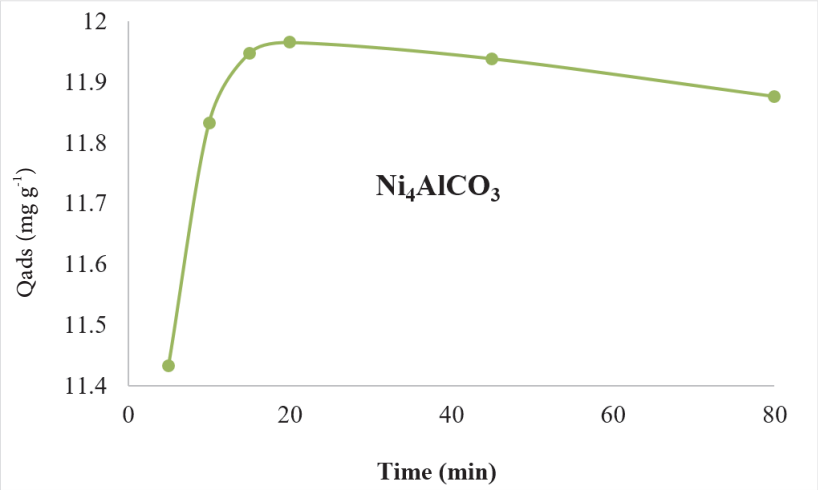

Fig. 7. Retention kinetics of Pb^{2+} on anionic clays studied

3.3. Kinetic models of adsorptions

To determine the most appropriate kinetic model, we have chosen three models, the most used for modelling adsorption kinetic data, which are: the pseudo-first-order (Equation 5), the second-order (Equation 6), and the intraparticle diffusion model (Equation 7). The corresponding equations in linear forms are presented as follows [28, 29].

$$\ln(q_e - q_t) = lnq_e - k_1.t \quad \text{(Eq.5)}$$

$$\frac{t}{q_t} = \frac{1}{k_2 q_e^2} + \frac{t}{q_e} \quad \text{(Eq.6)}$$

$$q_t = k_i t^{0.5} + C \quad \text{(Eq.7)}$$

Where q_e, q_t, t, k_1, k_2, k_i, and C are respectively the quantity of Pb^{2+} adsorbed at equilibrium (mg g^{-1}), the quantity of Pb^{2+} adsorbed at time t (mg g^{-1}), the time (min), the rate constant of the pseudo-first-order kinetic equation in g/mg min^{-1}, the rate constant of the pseudo-second-order kinetic equation in g/mg min^{-1}, the rate constant mg/g$min^{0.5}$, and the boundary layer thickness.

3.3.1.Pseudo first-order model.

The calculated results of the pseudo-first-order equation are presented in Table 1 and Figure 8. The values of the correlation coefficients are low, and the values of qe acquired by this method are contrasted with the experimental values. So, adsorption cannot be classified as pseudo-first order.

Table 1. Pseudo-first-order model parameters

Clay	Parameters
Mg_3AlCO_3	q_e (mg g^{-1}) exp = 12.00 q_e (mg g^{-1}) cal = 0.048 K_1 (mg $g^{-1}min^{-1}$) = 0.00057 R^2 = 0.00025
Ni_2AlCO_3	q_e (mg g^{-1}) exp = 11.96 q_e (mg g^{-1}) cal = 0.51 K_1 (mg $g^{-1}min^{-1}$) = 0.06 R^2 = 0.13
Ni_3AlCO_3	q_e (mg g^{-1}) exp =11.86 q_e (mg g^{-1}) cal =0.44 K_1 (mg $g^{-1}min^{-1}$) = 0.018 R^2 = 0.38
Ni_4AlCO_3	q_e (mg g^{-1}) exp =11.93 q_e (mg g^{-1}) cal = 0.11 K_1 (mg $g^{-1}min^{-1}$) = 0.025 R^2 = 0.072

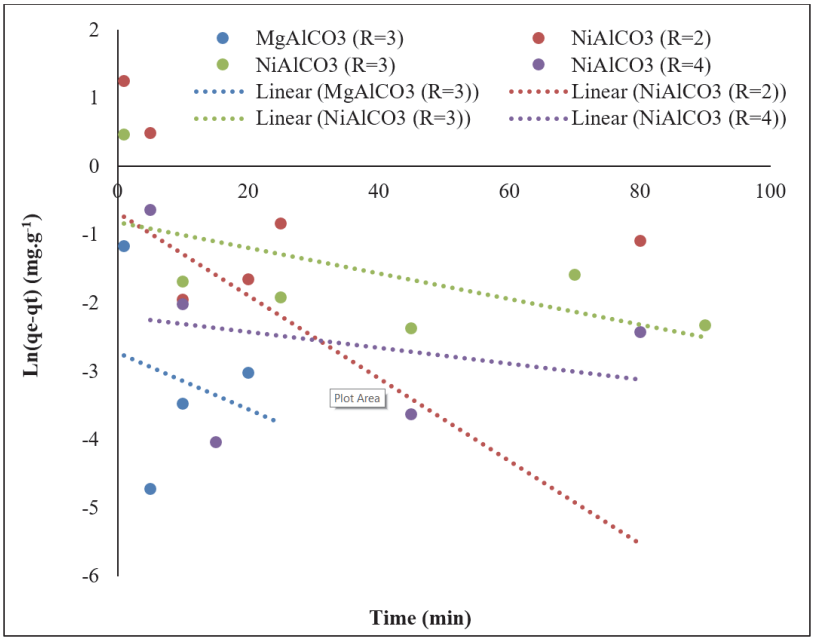

Fig. 8. Pseudo first-order model for anionic clays

3.3.2. Pseudo second-order model.

This model considers that the rate-limiting step in heavy metal adsorption is chemisorption and that chemisorptive bonds involving electron sharing or exchange between the absorbent and the adsorbent have been applied [5]. According to the high values of the regression constant R^2 = 0.99 for all the studied clays, the evolution of t/qt vs. t is presented by pseudo-second-order kinetics (Fig. 9). The parameters of the two kinetic models are shown in Table 2. From these results and in contrast to the first-order model, the amount of Pb^{2+} adsorbed at equilibrium determined experimentally is closer to that calculated using the second-order kinetic model (Table 2).

Table 2. Parameters of the pseudo-second-order model.

Clay	Parameters
Mg_3AlCO_3	q_e (mg g^{-1}) exp = 12.00 q_e (mg g^{-1}) cal =12.00 K_1 (mg $g^{-1}min^{-1}$) =-9.29 R^2 =1
Ni_2AlCO_3	q_e (mg g^{-1}) exp = 11.96 q_e (mg g^{-1}) cal = 11.93 K_2 (mg $g^{-1}min^{-1}$) = 0.487 R^2 = 0.99
Ni_3AlCO_3	q_e (mg g^{-1}) exp =11.86 q_e (mg g^{-1}) cal = 11.88 K_2 (mg $g^{-1}min^{-1}$) = 1.59 R^2= 0.99
Ni_4AlCO_3	q_e (mg g^{-1}) exp =11.93 q_e (mg g^{-1}) cal = 11.94 K_2 (mg $g^{-1}min^{-1}$) = 12.87 R^2 = 0.99

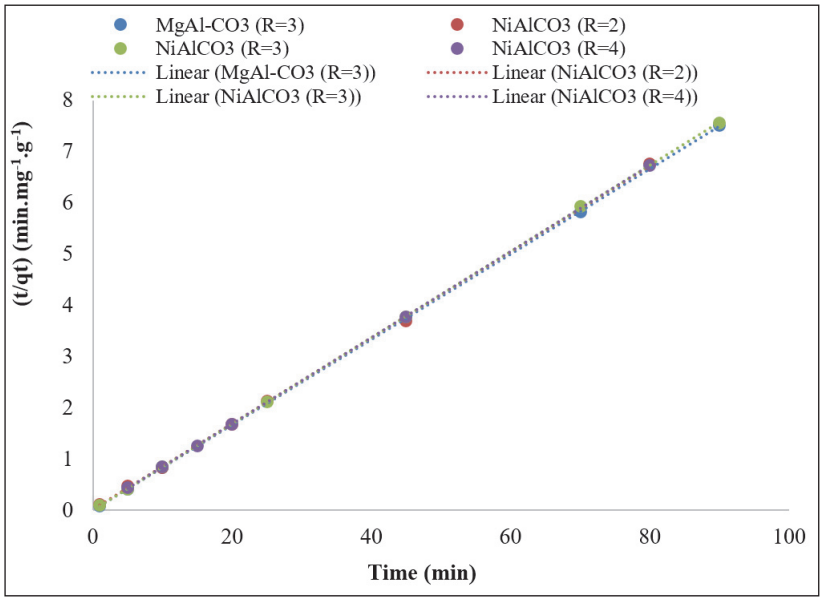

Fig. 9. Pseudo second-order model for anionic clays

3.3.3. Weber - Morris internal diffusion model

The Weber-Morris intra-particle diffusion model is the most used technique to identify the mechanism involved in the adsorption process. Intra-particle diffusion plots (q_t vs. $t^{0.5}$) (Fig. 10) were obtained from Equation 7. All the parameters of this model are presented in Table 3. Figure 10 indicates that straight lines do not pass through the point of origin before reaching the equilibrium state; therefore, the adsorption does not follow only the mechanism of intra-particle diffusion and that several processes affect the adsorption of Pb^{2+} and that intra-particle diffusion is not the limiting step for the whole reaction. The values of the constant C, which presents the thickness of the boundary layer, are in the order $C_{Mg3AlCO3} > C_{Ni2AlCO3} > C_{Ni3AlCO3} > C_{Ni4AlCO3}$. The values of C determine the boundary layer effect; higher values indicate a more significant impact [29].

Table 3. Parameters of the intra-particle diffusion model.

Clay	Parameters
Mg_3AlCO_3	$K_d = 0.135$ $C = 11.63$ $R^2 = 0.76$
Ni_2AlCO_3	$K_d = 1.54$ $C = 7.12$ $R^2 = 0.99$
Ni_3AlCO_3	$K_d = 0.68$ $C = 9.95$ $R^2 = 0.72$
Ni_4AlCO_3	$K_d = 0.32$ $C = 10.74$ $R^2 = 0.94$

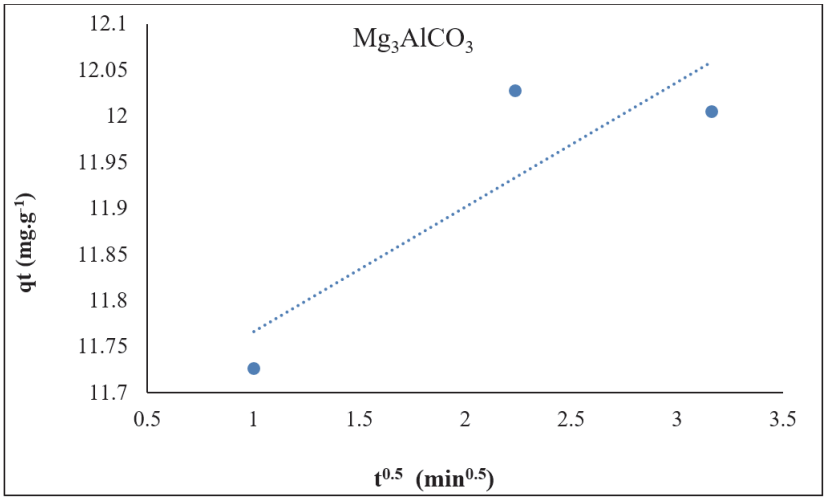
Mg3AlCO3
12.1
12.05
12
11.95
11.9
11.85
11.8
11.75
11.7
qt (mg.g-1)
0.5
1
1.5
2
2.5
3
3.5
t0.5 (min0.5)

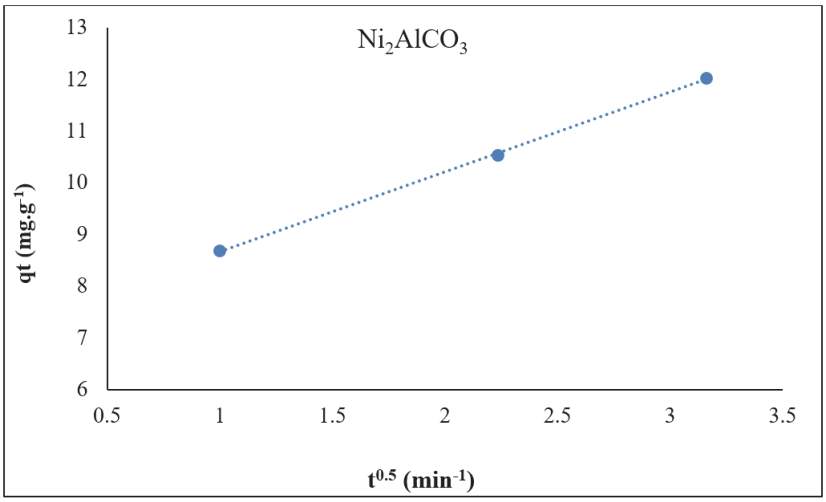
Ni2AlCO3
13
12
11
10
9
8
7
6
qt (mg.g-1)
0.5
1
1.5
2
2.5
3
3.5
t0.5 (min-1)

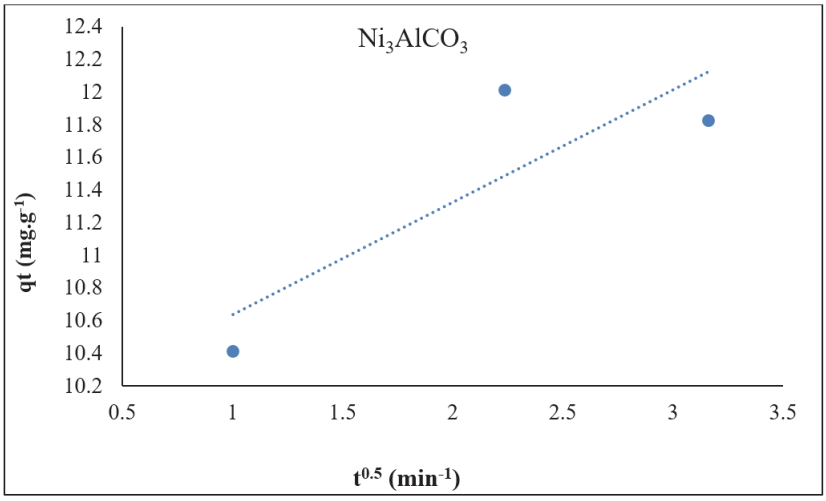
Ni3AlCO3
12.4
12.2
12
11.8
11.6
11.4
11.2
11
10.8
10.6
10.4
10.2
qt (mg.g-1)
0.5
1
1.5
2
2.5
3
3.5
t0.5 (min-1)

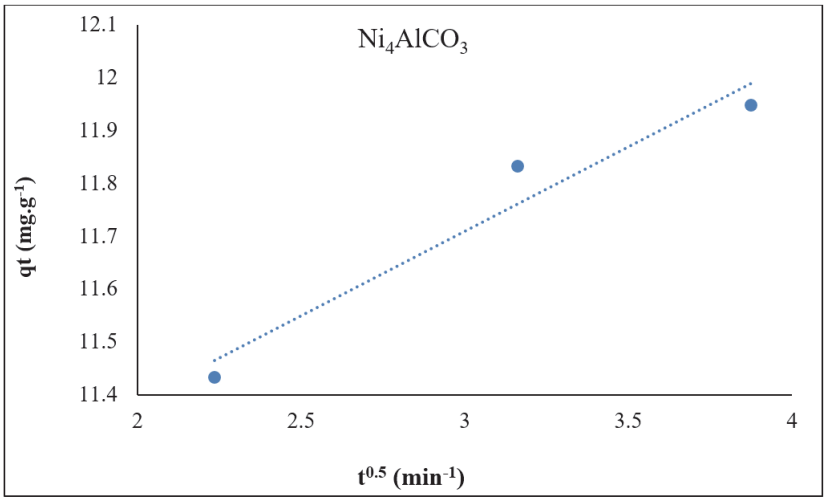

Fig. 10. Internal diffusion curves at a time less than 10 min

3.4. Lead retention equilibrium studies

To determine the adsorption characteristics of Mg_3AlCO_3 and $NiAlCO_3$ (R = 2, 3, and 4), a series of experiments are carried out in which solutions containing known concentrations of Pb^{2+} are in contact with the adsorbent. This study was carried out under the same conditions as the contact effect parameter, except for the concentrations of the Pb^{2+} solutions. After 24 hours, the solution concentration is measured when equilibrium has been established.

Figure 11 shows the curves of adsorbed amounts versus equilibrium concentrations for Pb^{2+} adsorption isotherms on Mg_3AlCO_3, Ni_2AlCO_3, Ni_3AlCO_3, and Ni_4AlCO_3 clays. The adsorption capacities of these clays are proportional to the metal concentrations. According to Giles et al., the allure of the isotherms is of type L [30]. Furthermore, the results showed that Mg_3AlCO_3 clay has a higher adsorption capacity than $NiAlCO_3$ (R = 2, 3, and 4).

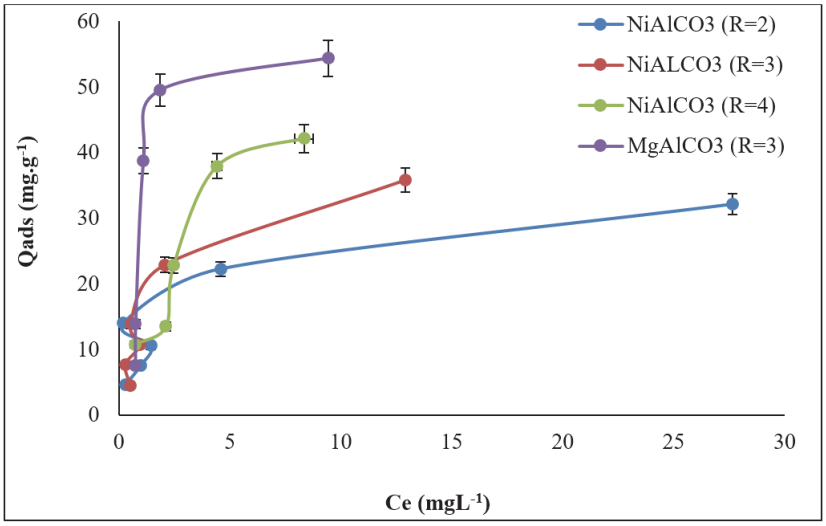

Fig. 11. Adsorption isotherms of Pb^{2+} on anionic clays studied.

3.4.1. Characterization of adsorbents before and after lead adsorption and mechanism

The infrared (IR) spectra of the raw Mg_3AlCO_3 and Ni_3AlCO_3 samples before and after the retention of lead at different concentrations are shown in Figure 12. The spectra are subdivided into three regions: between (1000 cm^{-1} and 400 cm^{-1}), (3000 cm^{-1} and 1000 cm^{-1}), and (4500 cm^{-1} and 3000 cm^{-1}). It can be noted that the IR spectra corresponding to the second region (1000 cm^{-1} to 3000 cm^{-1}) indicate two essential bands between (1650 cm^{-1} and 1660 cm^{-1}) and (1350 cm^{-1} and 1400 cm^{-1}) for both adsorbents before and after Pb^{2+} adsorption. These two bands are assigned to H2O and CO32-vibration modes, respectively. In the low-frequency region between 1000 cm^{-1} and 400 cm^{-1}, the infrared spectra after lead adsorption show intense vibration bands and are shifted compared to those of Mg_3AlCO_3 and Ni_3AlCO_3 before adsorption, as shown in Figure 12(a, b, c). For Mg_3AlCO_3, the vibration bands observed at 446.49 cm^{-1} and 554.49 cm^{-1} are attributed to the AlOH and MgOH bands, respectively [31]. After adsorption of the lead at different concentrations, the intensity of these bands increases and shifts slightly to high-frequency regions (447.49 cm^{-1} and 555.50 $cm^{-1,}$ respectively), which is explained by the fixation of Pb^{2+} ions on the lamellar layers to form bands of Pb-Al-OH and Pb-Mg-OH or M-O-Pb [32]. The band observed at 668.28 cm^{-1} for the Mg/Al-based clay before adsorption is assigned to the carbonate vibration mode [33]. After adsorption of Pb^{2+}, the spectrum does not show a remarkable shift of this band. The same remark was observed at the carbonate vibration band located at about 1357.79 cm^{-1} (Figure 12b) (second region). For the high-frequency region between (4500-3000 cm^{-1}), the vibration band of free hydroxyl groups located around 3446.55 cm^{-1} before adsorption is shifted to 3442 cm^{-1} for Mg_3AlCO_3 solids after lead adsorption for different concentrations. This shift, accompanied by the decrease of free OH band area after adsorption, is explained by the reduction of free OH in the hydroxyl layer, which reacts with Pb^{2+} ions according to Equation 8.

$$M\text{-}OH + Pb^{2+} \rightarrow M\text{-}O\text{- - -}Pb^{2+} + H^{+} \quad \text{(Eq. 8)}$$

As Equation 8, M is a divalent or trivalent cation (Mg or Al). For the adsorbent based on Ni_3AlCO_3, several bands were observed in the low-frequency region of the spectrum (<600 cm^{-1}) that characterize the lattice vibration modes [32]. The spectra indicate a slight shift with increasing peak intensity (sharp peak) at about 418.56 cm^{-1} for all Ni/Al-based HDLs after Pb^{2+} adsorption (Figure 12a). This band can be attributed to the formation of Al-O-Pb or Pb-Al-OH [32]. The infrared spectra also show the shift of the vibration band peaks from about 560.28 cm^{-1} and 594.99 cm^{-1} before adsorption to 562.25 cm^{-1} and 592.15 $cm^{-1,}$ respectively, for all Ni_3AlCO_3 clays after lead adsorption. The band's shift around 562 cm-1 has been assigned to hydroxyl groups associated with mainly Al [34], and bounds around 592 cm-1 have been given as hydroxyl groups associated with Al/Ni. The shift of these two bonds is assigned to the formation of M-O-Pb according to the reaction proposed above (case of Mg_3AlCO_3) (M = Ni^{2+} or Al^{3+}) [32]. Before the adsorption of Pb^{2+}, the strong and broad absorption band centred on 3483.20 cm^{-1} corresponds to the O–H stretching vibration of the layer surface and interlayer water molecules, and the band in 1652.88 cm^{-1} is due to the O–H bending vibration of water molecules. After adsorption of the lead, we notice the reduction and slight shift of the bands, which are centred towards a low frequency at 3482.53 cm^{-1}, indicating that the hydroxyl groups electrostatically attracted Pb^{2+} anions.

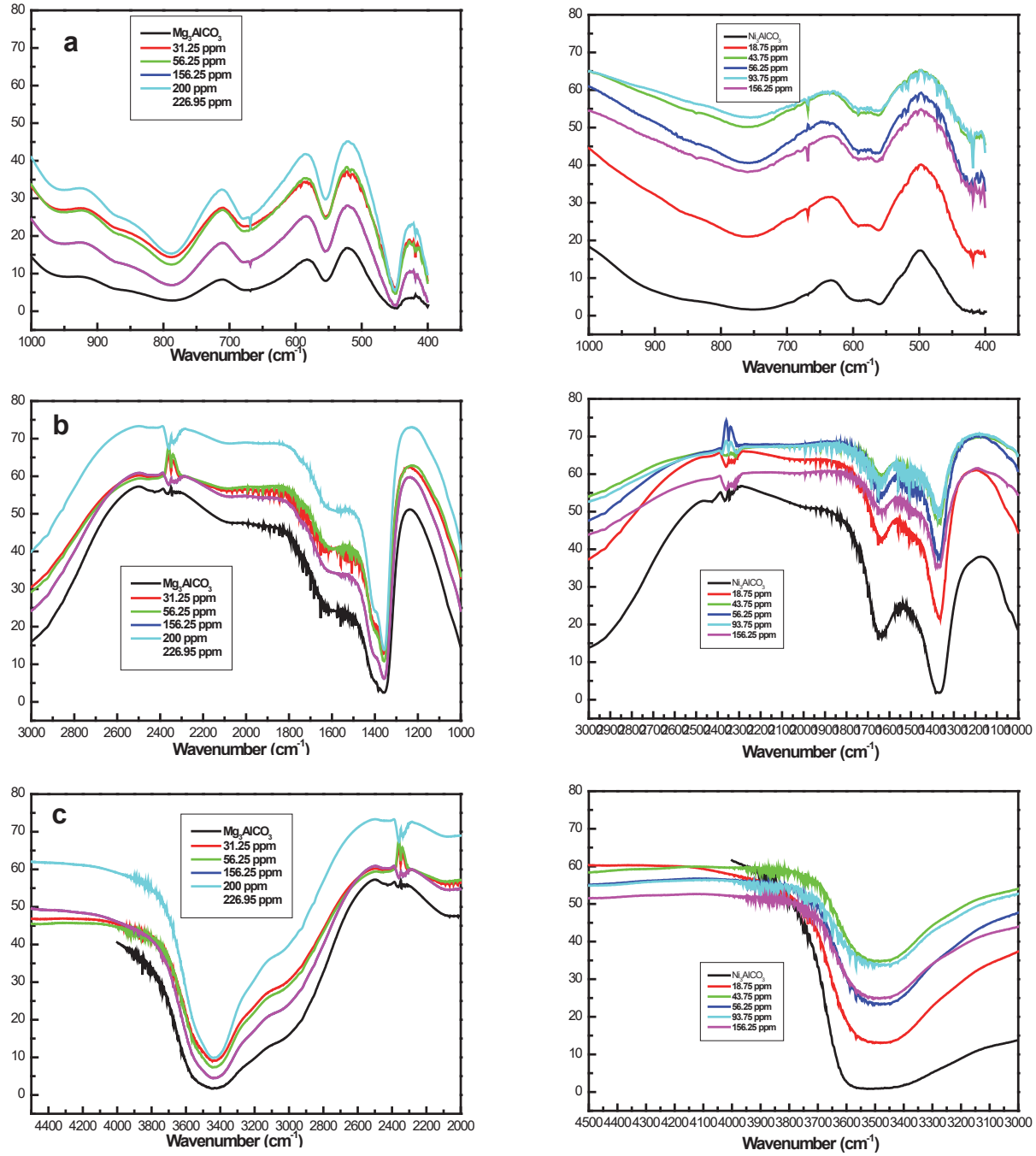

Fig. 12. FT-IR spectra of Mg_3AlCO3 and Ni_3AlCO_3 before and after uptake of lead at different concentrations. (a) region to 1000 cm^{-1} to 400 cm^{-1}, (b) region to 3000 cm^{-1} at 1000 cm^{-1}, and (c) region to 4500 cm^{-1} to 3000 cm^{-1}

3.4.2.Model of adsorption isotherms

Modelling adsorption isotherm data is essential for predicting and comparing adsorption performance. Lead (Pb) adsorption was modelled using Langmuir, Freundlich, and Temkin models. The linear equations that correspond to the three models are presented in Equations 9, 10, and 11 [28, 35].

$$\frac{C_e}{q_e} = \frac{1}{q_m K_L} + \frac{C_e}{q_m} \quad \text{(Eq. 9)}$$

$$\ln q_e = \frac{1}{n}\ln C_e + \ln(7) \quad \text{(Eq. 10)}$$

$$q_e = B.\ln A + B \quad \text{(Eq. 11)}$$

Where C_e, q_e, and q_m (mg g^{-1}) are the equilibrium concentration of lead (mg g^{-1}), the quantity of Pb^{2+} adsorbed at equilibrium (mg g^{-1}), and the maximum monolayer adsorption capacity of adsorbent (mg g^{-1}), respectively. n and K_F are the Freundlich adsorption constants. K_L is the Langmuir adsorption constant (Lmg^{-1}). This last parameter is used to calculate the dimensionless equilibrium parameter (R_L) that explains the favorability of the adsorption process; R_L is calculated from Equation 12 [35].

$$R_L = \frac{1}{1 + K_L C_0} \quad \text{(Eq. 12)}$$

B is a constant related to the heat of adsorption, which equals B = RT/b. R, T, and b are the gas constant (8.314 $J.mol^{-1} K^{-1}$), the absolute temperature (K), and the Temkin constant ($J\ mol^{-1}$). Typical adsorption isotherms for Pb^{2+} on all selected anionic clays are shown in Figures 13, 14 and 15, respectively, for the Langmuir, Freundlich, and Temkin models.

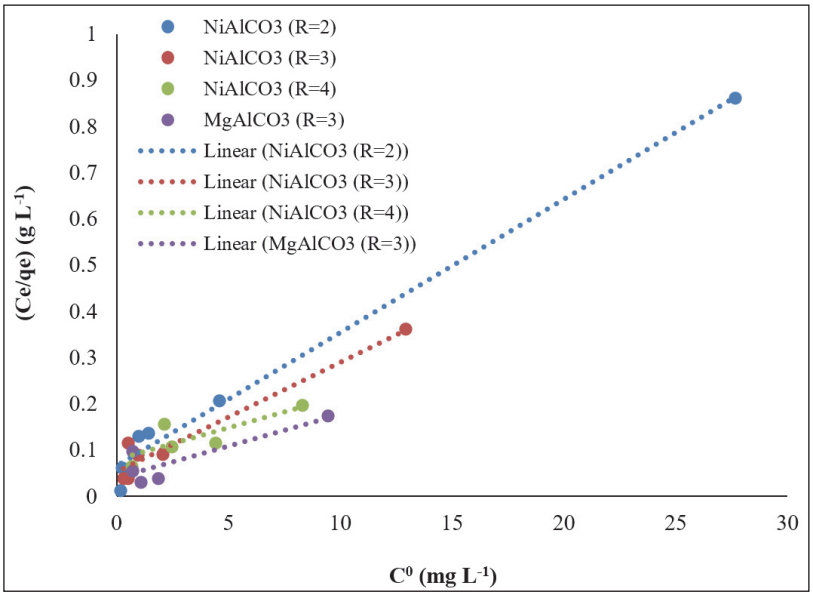

Fig. 13. Langmuir isotherm model of the studied anionic clays

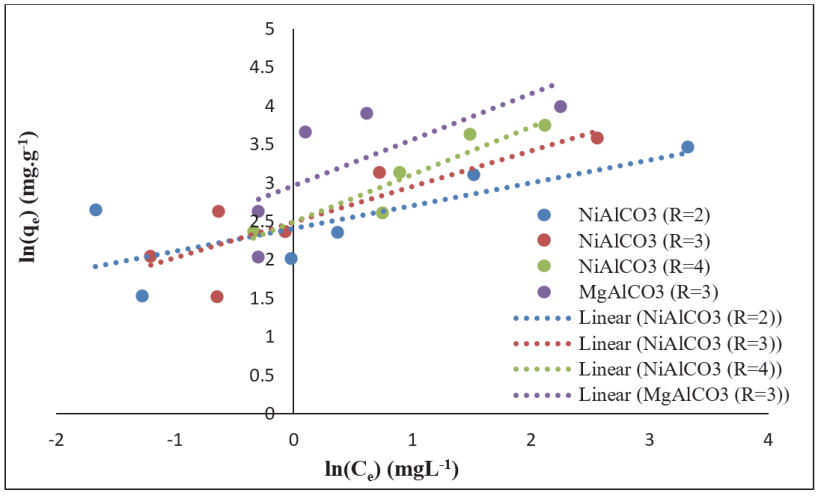

Fig. 14. Freundlich isotherm model of the studied anionic clays

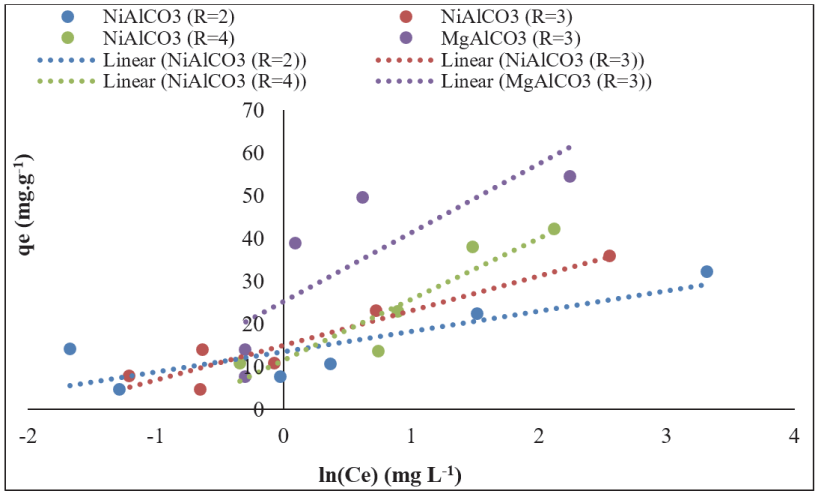

Fig. 15. Temkin isotherm model of the studied anionic clays

According to Figures (12 and 14) and the regression coefficients found and shown in Table 4, the Pb^{2+} adsorption data on all the anionic clays followed the Langmuir and Temkin models. The values of the equilibrium parameter without dimension R_L are between 0 and 1 for all the studied clays, showing that the adsorption of lead is favourable (Table 4).

The lead adsorption capacity values (Qm) found from the Langmuir model show that Mg_3AlCO_3 has a large adsorption capacity (73.42 mg g^{-1}). For Ni/Al-based clays, the Pb^{2+} ions adsorption capacity increases with the increase of the molar ratio, and Ni_4AlCO_3 has a Pb^{2+} adsorption capacity close to Mg_3AlCO_3.

Table 4. Parameters of Pb^{2+} adsorption isotherm models on selected anionic clays

Langmuir	**q_{max} (mg g^{-1})**	**b (L mg^{-1})**	**R_L**	**R^2**
Mg_3AlCO_3	73.42	0.33	0.04	0.73
Ni_2AlCO_3	35.71	0.44	0.05	0.98
Ni_3AlCO_3	43.47	0.44	0.05	0.95
Ni_4AlCO_3	72.51	0.17	0.07	0.66
Freundlich	**K_f**	**(n)**		**R^2**
Mg_3AlCO_3	19.29	1.67		0.52
Ni_2AlCO_3	11.14	3.37		0.60
Ni_3AlCO_3	12.05	2.15		0.72
Ni_4AlCO_3	12.08	1.62		0.95
Temkin	**K_t(L mg^{-1})**	**b**	**B_T (j mol^{-1})**	**R^2**
Mg_3AlCO_3	1.00	155.14	16.13	0.66
Ni_2AlCO_3	16.96	527.95	4.74	0.85
Ni_3AlCO_3	6.35	309.33	8.09	0.89
Ni_4AlCO_3	2.24	176.35	14.19	0.85

According to the correlation coefficients of the Freundlich model, the total experimental data on lead adsorption on anionic clays do not follow the Freundlich model (Table 4). The n value in the range of 1.62–3.37 indicates a favourable adsorption process. The correlation coefficients for the Temkin model of all the clays studied show that this last model adequately represents the experimental data on lead adsorption. The Temkin constant (BT) values presented in Table 4, related to the heat of sorption of Pb^{2+}, increase with the increase of the molar ratio of Ni/Al.

3.5. Thermodynamic parameters

To describe the thermodynamic behaviour of the absorption of Pb^{2+} ions in the aqueous solution, we use the following Equation13 and 14 [35, 36].

$$\ln K_D = \frac{-\Delta H}{RT} + \frac{\Delta S}{R} \quad \text{(Eq.13)}$$

$$\Delta G = -RT \ln K_D \quad \text{(Eq.14)}$$

where ΔH, ΔS, ΔG and T are the enthalpy, entropy, Gibbs free energy, and absolute temperature, respectively, and R is the gas constant (8.314 J k^{-1}. mol^{-1}), $K_D = (q_e/C_e)$, which depends on temperature. The thermodynamic parameters are determined starting from the lines of ln (k_D) vs. (1/T) in the linear domain of temperature, corresponding to the adsorption of lead, i.e., between 20°C and 50°C. The thermodynamic parameters are presented in Table 5. The positive values of enthalpy suggested the endothermic nature of the adsorption. They reflected the affinity of the adsorbent for Pb^{2+} ions [36]. The low H values for both adsorbents are 17.39 KJ mol^{-1} for Mg_3AlCO_3 and 4.97 for Ni_3AlCO_3, which are less than 40 KJ mol^{-1}. It shows a physical adsorption between Pb^{2+} ions and these clays [37]. Positive entropy values showed that the randomness at the solute-solution interface increases with the adsorption of Pb^{2+} in the adsorption process. Negative free energy values indicate a spontaneous process of the adsorption of Pb^{2+} by Mg_3AlCO_3 and Ni_3AlCO_3. These results obtained for Mg_3AlCO_3 agree with those found by Ayawei et al. [38].

4. Conclusion

As part of the study of layered double hydroxides and the possibility of using them as adsorbents to remove lead from water, we have synthesized in our laboratory two types of anionic clays by the direct co-precipitation method, namely Mg_3AlCO_3 and Ni_3AlCO_3. The analysis techniques used to characterize the LDHs show that the synthesized clays are materials from the family of layered double hydroxides. They have the same properties as the anionic clays of the Mg_3AlCO_3 and Ni_3AlCO_3 types. The pH, adsorbent mass, temperature, contact time, and molar ratio show that the adsorption capacity of Pb^{2+} by Mg_3AlCO_3 is higher than that of Ni_3AlCO_3. According to the Langmuir model,

Table 5. Thermodynamic parameters for the adsorption of Pb^{2+} by Mg_3AlCO_3 and Ni_3AlCO_3 at various temperatures

Adsorbent	ΔS (KJ.K^{-1}.mol^{-1})	ΔH (KJ.mol^{-1})	Temperature			
			298 K	303 K	313K	323 K
			K_d			
Mg_3AlCO_3	0.065	17.39	2.32	2.90	2.72	4.02
			ΔG (KJ.mol^{-1})			
			-2,08	-2.68	-3.42	-3.74
			K_d			
Ni_3AlCO_3	0.018	4.97	1.261	1.265	1.363	1.461
			ΔG (KJ.mol^{-1})			
			-0.576	-0.594	-0.80	- 0.102

Ni_4AlCO_3 and Mg_3AlCO_3 clays have a high lead adsorption capacity, and the maximum adsorption capacity values are 72.51mg g^{-1} and 73.42 mg g^{-1} for Ni_4AlCO_3 and Mg_3AlCO_3, respectively. At an optimal pH of 6.5, the removal percentages reach 95.4 % and 81.3 % for Mg_3AlCO_3 and Ni_3AlCO_3, respectively. The adsorbed amount increases with increasing temperature for both types of LDHs, where the lead removal percentages reach 94.16 % and 85.39 % for Mg_3AlCO_3 and Ni_3AlCO_3, respectively, and the adsorption capacities of Pb^{2+} were obtained ($Q_{Ni4AlCO3} > Q_{Ni3AlCO3} > Q_{Ni2AlCO3}$). The results showed that at pH below 6.5, the removal of Pb^{2+} may be achieved by complexation reactions, and the lead precipitated at higher pH. The experimental data on lead adsorption kinetics show that the pseudo-second-order model best describes the adsorption kinetics. The results of the applied Pb^{2+} adsorption isotherm models indicate that the Langmuir and Temkin models are the most adequate to represent the experimental data for both adsorbents. In addition, thermodynamic parameters show that the adsorption of lead by Mg_3AlCO_3 and Ni_3AlCO_3 is endothermic, spontaneous and random at the solute-solution interface.

5. Acknowledgements

The authors would like to thank the MESRS and DGRSDT (Ministère de l'Enseignement Supérieur et de la Recherche Scientifique et la Direction Générale de la Recherche Scientifique et du Développement Technologique- Algérie) for their Financial support.

6. Conflict of interest

We have no conflicts of interest to disclose.

7. References

[1] T.V. Toledo, C.R. Bellato, K.D. Pessoa, M.P. Fontes, Magnetic compounds based in hydrotalcites for removal of anionic contaminants in water, Quim. Nova., 36 (2013) 419–425. http://doi.org/10.1590/S0100-40422007000500005.

[2] M. Bouraada, F. Belhalfaoui, M.S. Ouali, Sorption study of an acid dye from an aqueous solution on modified Mg–Al layered double hydroxides, J. Hazard. Mater., 163 (2009) 463–467. http://doi.org/ 10.1016/j.jhazmat.2008.06.108

[3] L. D. Miranda, C. R., Bellato, M. P. Fontes, M. F. de Almeida, J. L. Milagres, L. A. Minim, Preparation and evaluation of hydrotalcite-iron oxide magnetic organocomposite intercalated with surfactants for cationic methylene blue dye removal, Chem. Eng. J., 254 (2014) 88-97. http://doi.org/10.1016/j.cej.2014.05.094

[4] R. Shi, P. Yangn, Y. Yin, X. Dong, J. Li. Fabrication of porous microspheres and network arrays of Zn–Al hydrotalcite-like compounds on Al substrate via facile hydrothermal method, Ceram. Int., 40 (2014) 6855–6863. http://doi.org/10.1016/j.ceramint.2013.12.005.

[5] E. Ramos-Ramírez, N. L. Gutiérrez Ortega, C. A. Contreras Soto, M. T. Olguín Gutiérrez, Adsorption isotherm studies of chromium (VI) from aqueous solutions using sol–gel hydrotalcite-like compounds, J. Hazard. Mater., 172 (2009) 1527–1531. http://doi.org/10.1016/j.jhazmat.2009.08.023

[6] S. V. Prasanna, P. V. Kamath, Anion-exchange reactions of layered double hydroxides: interplay between coulombic and H-bonding interactions, Ind. Eng. Chem. Res., 48 (2009) 6315-6320. http://doi.org/10.1021/ie9004332

[7] A. V. Radha, P. V. Kamath, C. Shivakumara, Mechanism of the anion exchange reactions of the layered double hydroxides (LDHs) of Ca and Mg with Al, Solid State Sci., 7 (2005) 1180-1187. http://doi.org/10.1016/j.solidstatesciences.2005.05.004

[8] M. Lakraimi, A. Legrouri, A. Barroug, A. DeRoy and J. P. Besse, Preparation of a new stable hybrid material by chloride–2,4-dichlorophenoxyacetate ion exchange into the zinc–aluminium–chloride layered double hydroxide, J. Mater. Chem., 10 (2000) 1007-1011. http://doi.org/10.1039/A909047I

[9] N. Drici. Hydroxydes doubles lamellaires, synthèse, caractérisation et propriétés.

Matériaux. Université Sorbonne Paris Cité, Français, NNT: 2015USPCD007, 2015. https://theses.hal.science/tel-01488539v1/file/edgalilee_th_2015_drici.pdf

[10] E. Géraud, V. Prévot, J. Ghanbaja, F. Leroux, Macroscopically ordered hydrotalcite-type materials using self-assembled colloidal crystal template, Chem. Mater., 18 (2006) 238–240. http://doi.org/10.1021/cm051770i

[11] K. Kadirvelu, M. Kavipriya, C. Karthika, M. Radhika, N. Vennilamani, S. Pattabhi, Utilization of various agricultural wastes for activated carbon preparation and application for the removal of dyes and metal ions from aqueous solutions, Bioresour. Technol., 87 (2003) 129-32. http://doi.org/10.1016/s0960-8524(02)00201-8.

[12] A. K. Jain, V. K. Gupta, A. Bhatnagar, Utilization of industrial waste products as adsorbents for the removal of dyes, J. Hazard. Mater., 101 (2003) 31-42. http://doi.org/10.1016/s0304-3894(03)00146-8.

[13] Y. Yasin, M. Mohamad, A. Saad, A. Sanusi, F. H. Ahmad, Removal of lead ions from aqueous solutions using intercalated tartrate-Mg–Al layered double hydroxides, Desalin. Water Treatment., 52 (2014) 4266-4272. http://doi.org/10.1080/19443994.2013.803935

[14] S. Yanming, L. Dongbin, L. Shifeng, F. Lihui, C. Shuai, M. A. Haque, Removal of lead from aqueous solution on glutamate intercalated layered double hydroxide, Arab. J. Chemy., 10 (2017) S2295-S2301. http://doi.org/10.1016/j.arabjc.2013.08.005.

[15] E. J. Pacer, C. D. Palmer, P. J. Parsons, Determination of lead in blood by graphite furnace atomic absorption spectrometry with Zeeman background correction: Improving a well-established method to support a lower blood lead reference value for children, Spectrochim. Acta Part B: Atom. Spect., 190 (2022) 106324. http://doi.org/10.1016/j.sab.2021.106324

[16] M. S. Tudosie, G. Caragea, D. M. Popescu, O. Avram, D. Serban, C. G. Smarandache, A. M. Dascalu, Optimization of a GF AAS method for lead testing in blood and urine: A useful tool in acute abdominal pain management in emergency, Exp. Ther. Med., 22 (2021) 1-8. http://doi.org/10.3892/etm.2021.10417.

[17] ZW. Zhang, S. Shimbo, N. Ochi, M. Eguchi, T. Watanabe, CS. Moon, M. Ikeda, Determination of lead and cadmium in food and blood by inductively coupled plasma mass spectrometry: a comparison with graphite furnace atomic absorption spectrometry, Sci. Total Environ., 205 (1997) 179-87. http://doi.org/10.1016/s0048-9697(97)00197-6.

[18] M. Trzcinka-Ochocka, R. Brodzka, B. Janasik, Useful and fast method for blood lead and cadmium determination using ICP-MS and GF-AAS; validation parameters, J. Clin. Lab. Anal., 30 (2016) 130-9. http://doi.org/10.1002/jcla.21826.

[19] D. Fuger, Mise en application de processus analytique complexe Analyse de métaux par ICP-AES. Robert Schuman–Département chimie, Université de Strasbourg, France, 2011. https://www.chemphys.fr/mpb/teach/ICP-AES/ICP-AES.pdf

[20] R. Riyanto, Determination of lead in waste water using cyclic voltammetry by platinum wire electrode, J. Sci. Data Anal., 14 (2014) 22-33. http://doi.org/10.20885/eksakta.vol14.iss2.art3.

[21] F. Delorme, A. Seron, M. Bizi, V. Jean-Prost, D. Martineau. Effect of time on the reconstruction of the $Mg_4Al_2(OH)1_2CO_3.3H_2O$ layered double hydroxide in a Na_2CO_3 solution, J. Mater. Sci., 41 (2006) 4876-4882. http://doi.org/10.1007/s10853-006-0304-4

[22] K. Klemkaite, I. Prosycevas, R. Taraskevicius, A. Khinsky, A. Kareiva, Synthesis and characterization of layered double hydroxides with different cations (Mg, Co, Ni, Al), decomposition and reformation of mixed metal oxides to layered structures, Open Chem., 9 (2011) 275-282. http://doi.org/10.2478/s11532-011-0007-9

[23] A. Faour, C. Mousty, V. Prevot, B. Devouard,

A. De Roy, P. Bordet, C. Taviot-Gueho, Correlation among structure, microstructure, and electrochemical properties of NiAl–CO_3 layered double hydroxide thin films, J. Phys. Chem. C, 116 (2012) 15646-15659. http://doi.org/10.1021/jp300780w

[24] F. Cavani, F. Trifiro, A Vaccari, Hydrotalcite-type anionic clays: Preparation, properties and applications, Catal. Today, 11 (1991) 173-301. http://doi.org/10.1016/0920-5861(91)80068-K

[25] L. Xuefeng, H. Wanguo, X. Yingming, Sorption of lead ion by layered double hydroxide intercalated with diethylenetriaminepentaacetic acid, Colloids Surf. A Physicochem. Eng. Asp., 366 (2010) 50-57. http://doi.org/10.1016/j.colsurfa.2010.05.012

[26] D. Zhao, G. Sheng, J. Hu, C. Chen, X. Wang, The adsorption of Pb (II) on Mg_2Al layered double hydroxide, Chem, Eng, J., 171 (2011) 167-174. http://doi.org/10.1016/j.cej.2011.03.082.

[27] M. Arshadi, M. J. Amiri, S. Mousavi, Kinetic, equilibrium and thermodynamic investigations of Ni (II), Cd (II), Cu (II) and Co (II) adsorption on barley straw ash, Water Resour. Ind., 6 (2014) 1-17. http://doi.org/10.1016/j.wri.2014.06.001

[28] J. B. Huo, G. Yu, Layered double hydroxides derived from MIL-88A (Fe) as an efficient adsorbent for enhanced removal of lead (II) from water, Int. J. Mol. Sci., 23 (2022) 14556. http://doi.org/10.3390/ijms232314556

[29] G. W. Kajjumba, S. Emik, A. Öngen, H. K. Özcan, S. Aydın, Modelling of adsorption kinetic processes—errors, theory and application, Advanced Sorption Process Applications, page 1-19, 2018. http://doi.org/10.5772/intechopen.80495

[30] C. H. Giles, T. H. MacEwan, S. N. Nakhwa, D. Smith, Studies in adsorption. Part XI. A system of classification of solution adsorption isotherms, and its use in diagnosis of adsorption mechanisms and in measurement of specific surface areas of solids, J. Chem. Soc. Resumed., 32 (1960) 3973–3993. https://doi.org/10.1039/JR9600003973

[31] V. Rives, Layered double hydroxides: present and future, Nova Science Publishers, Inc., New York, 2001, http://doi.org/10.1016/S0169-1317(02)00112-6

[32] R. Marangoni, M. Bouhent, , C. Taviot-Gueho, F. Wypych, F. Leroux. Zn2Al layered double hydroxides intercalated and adsorbed with anionic blue dyes: A physico-chemical characterization, J. Colloid Interface Sci., 333 (2009) 120-127. http://doi.org/10.1016/j.jcis.2009.02.001

[33] T.N. Moroz, Formation of spinel from hydrotalcite-like minerals and destruction of chromite implanted by inorganic salts, App. Clay Sci., 18 (2001) 29–36. http://doi.org/10.1016/S0169-1317(00)00027-2

[34] P. Benito, I. Guinea, F. M. Labajos, V. Rives, Microwave-assisted reconstruction of Ni, Al hydrotalcite-like compounds, J. Solid State Chem., 181 (2008) 987-996. http://doi.org/10.1016/j.jssc.2008.02.003

[35] A. A. Inyinbor, F. A. Adekola, G. A. Olatunji, Kinetics, isotherms and thermodynamic modeling of liquid phase adsorption of Rhodamine B dye onto Raphia hookerie fruit epicarp, Water Resour. Ind., 15 (2016) 14-27. http://doi.org/10.1016/j.wri.2016.06.001

[36] J. X. Lin, S. L. Zhan, M. H. Fang, X. Q. Qian, H. Yang, Adsorption of basic dye from aqueous solution onto fly ash, J. Environ. Manage., 87 (2008) 193-200. http://doi.org/10.1016/j.jenvman.2007.01.001

[37] B. Houari, S. Louhibi, K. Tizaoui, L. Bouklihacene, B. Benguella, T. Roisnel, V. Dorcet, New synthetic material removing heavy metals from aqueous solutions and wastewater, Arab. J. Chem., 12 (2019) 5040-5048. http://doi.org/10.1016/j.arabjc.2016.11.010

[38] N. Ayawei, C. Y. Abasi, D. Wankasi, E. D. Dikio, Layered double hydroxide adsorption of lead: equilibrium, thermodynamic and kinetic studies, Int. J. Adv. Res. Chem. Sci., 2 (2015) 22-32. https://www.arcjournals.org/pdfs/ijarcs/v2-i5/3.pdf